ARTICLE NO. 79-0445R

C 80-052

# Influence of Ballonet Motions on the Longitudinal Stability of Tethered Aerostats

00017
00020
00024

James DeLaurier*
*University of Toronto, Toronto, Canada*

**To date tethered aerostat stability analyses have assumed the ballonet air to be "frozen" with respect to the rest of the aerostat. Also, it was assumed that the least stable, and hence most important, longitudinal mode of motion was the first mode, where the cable's and aerostat's motions are so coupled as to approximate an "upside-down pendulum." The present analysis shows that when motion of the internal air and gas is allowed, a third mode appears whose stability may be equal to, or less than, that of the first mode for current aerostat designs. The degree of the third mode's stability is primarily controlled by the ballonet's fore-and-aft constraint and damping, and current design practices applied to larger and higher altitude aerostats could give rise to systems with serious stability problems at lower altitudes. However, this investigation also shows that moderate increases in constraint and damping, which should be achievable by ballonet redesign, would strongly stabilize the third mode.**

## Nomenclature

$A$ = matrix of coefficients from the dynamic Eqs. (25)
$B$ = total buoyant force of the aerostat
$\bar{c}$ = characteristic length of the aerostat
$\hat{C}$ = damping coefficient defined by Eq. (23)
$c_a, c_g$ = damping coefficients of the hull's internal air and gas, respectively
$C_x, C_z$ = nondimensional aerodynamic forces in the $x$ and $z$ directions, respectively
$C_m$ = nondimensional aerodynamic moment about the $y$ axis
$dx_a/d\theta$ = axial ballonet constraint term used in Eq. (30)
$D(\ )$ = nondimensional time derivative, $(\bar{c}/2U_0)(\cdot)$
$E$ = matrix of coefficients from the dynamic Eqs. (25)
$f$ = ballonet fullness, %
$g$ = gravitational acceleration
$h$ = vertical body-fixed aerostat coordinate shown in Fig. 2
$I_{yy}, I_{zz}$ = moments of inertia about the $y$ and $z$ axes, respectively
$I_{xz}$ = product of inertia with respect to $x$ and $z$ axes
$\hat{K}$ = spring constant defined by Eq. (24)
$k_a, k_g$ = spring constants of the hull's internal air and gas, respectively
$l$ = axial body-fixed aerostat coordinate shown in Fig. 2
$L$ = total tether cable length (see Fig. 4)
$m$ = mass of the aerostat, excluding the hull's internal air and gas
$\hat{M}$ = equivalent mass term defined by Eq. (22)
$m_a, m_g$ = masses of the hull's internal air and gas, respectively
$N_{1/2}$ = number of cycles for unforced ballonet slosh to damp to half amplitude
$q$ = aerostat angular velocity about the $y$ axis
$\hat{q}$ = nondimensional $q$, $\bar{c}q/(2U_0)$
$\hat{Q}$ = complex eigenvector term for $q$ from Eq. (26)
$S$ = aerostat reference area
$t$ = time
$T$ = tether cable tension
$\hat{T}$ = complex eigenvector term for $\delta T$ from Eq. (26)
$\hat{U}$ = complex eigenvector term for $u$ from Eq. (26)
$u$ = velocity of the mass center of $m$ in the $x$ direction
$\hat{u}$ = nondimensional $u$, $u/U_0$
$U_0$ = mean wind speed
$v_a, v_g$ = mass center velocities of $m_a$ and $m_g$, respectively, with respect to the mass center of $m$ and in the $x$ direction
$V$ = volume
$\hat{V}_a$ = complex eigenvector term for $v_a$ from Eq. (26)
$w$ = velocity of the mass center of $m$ in the $z$ direction
$\hat{W}$ = complex eigenvector term for $w$ from Eq. (26)
$x, z$ = body-fixed coordinates (Fig. 4) originating at the mass center of $m$
$y$ = body-fixed coordinate normal to $x$ and $z$, and into the plane of Fig. 4
$X, Y, X$ = forces on $m$ in the $x, y$, and $z$ directions, respectively
$\hat{X}_a$ = complex eigenvector term for $\delta x_a$ from Eq. (26)
$\alpha$ = aerodynamic angle of attack, $w/U_0$
$\gamma$ = perturbed cable angle
$\Gamma$ = cable angle defined in Fig. 4
$\hat{\Gamma}$ = complex eigenvector term for $\gamma$ from Eq. (26)
$\delta(\ )$ = quantity perturbed from equilibrium
$\Delta(\ )$ = quantity perturbed from equilibrium
$\eta$ = real part of $\sigma$
$\theta$ = aerostat pitch angle defined in Fig. 4
$\hat{\theta}$ = complex eigenvector term for $\theta$ from Eq. (26)
$\rho$ = density of the air at the aerostat
$\sigma$ = stability root defined by Eqs. (26-28)
$\omega$ = imaginary part of $\sigma$

*Subscripts*

$a$ = with respect to internal air of the hull
aero = wind force (or moment) term
$B$ = with respect to the volumetric center of the aerostat's total displaced volume
$c$ = tether cable term
$cm$ = term pertaining to the mass center of $m$
$g$ = with respect to the lifting gas in the hull

Presented as Paper 79-0445 at the 6th AIAA Aerodynamic Decelerator and Balloon Technology Conference, Houston, Texas, March 5-7, 1979; submitted April 9, 1979; revision received Oct. 4, 1979. 

Index categories: Lighter-than-Airships; Handling Qualities, Stability and Control; Performance.

*Associate Professor, Institute for Aerospace Studies.

$o$ = reference equilibrium term
$q$ = derivative of $X$, $Z$, $M$ with respect to $q$; derivative of $C_x$, $C_z$, $C_m$ with respect to $\hat{q}$
$\dot{q}$ = derivative of $X$, $Z$, $M$ with respect to $\dot{q}$; derivative of $C_x$, $C_z$, $C_m$ with respect to $D\hat{q}$
$tp$ = with respect to the tether-cable confluence point
$u$ = derivative of $X$, $Z$, $M$ with respect to $u$; derivative of $C_x$, $C_z$, $C_m$ with respect to $\hat{u}$
$\dot{u}$ = derivative of $X$, $Z$, $M$ with respect to $\dot{u}$; derivative of $C_x$, $C_z$, $C_m$ with respect to $D\hat{u}$
$w$ = derivative with respect to $w$
$\dot{w}$ = derivative with respect to $\dot{w}$
$\alpha$ = derivative with respect to $\alpha$
$\dot{\alpha}$ = derivative with respect to $D\alpha$

*Superscript*

= derivative with respect to $t$

## Introduction

LARGE, nonrigid, aerodynamically shaped balloons, e.g., blimps and tethered aerostats, allow for the expansion of their lifting gas by means of a ballonet, which is an internal fabric envelope inflated with air. This air is pressurized by means of a blower fan (Fig. 1) and this pressure, in turn, is transmitted to the outer hull to establish its rigidity. As the gas expands from increasing altitude or temperature, the ballonet is correspondingly compressed and its air is valved to the atmosphere. Therefore, no gas is lost and the hull's internal pressure stays approximately constant. For balloons with design altitudes of 10,000 ft, the ballonet volume is approximately 35% of the total hull volume. Therefore, at low altitudes, the mass of the ballonet air is generally a sizeable percentage of the total balloon's mass ($\approx$20-40%).

Most dynamic analyses of tethered aerostats have assumed the ballonet air to be "frozen" with respect to the balloon's hull.[1-3] In reality, a partially filled ballonet "sloshes," relative to the lifting gas, in a manner similar to liquid slosh in a partially filled container.[4] The "frozen" ballonet assumption was an analytical convenience justified by the fact that the slosh frequency is generally an order of magnitude larger than that of the tethered aerostat system's least-stable mode, the "upside-down pendulum" mode.[2] It was thus assumed that there would be no significant coupling between these motions, which was subsequently verified by experiments in 1974[3] on a 200,000 ft$^3$ Family-II tethered aerostat (Fig. 2).

However, new aerostats have been envisioned which would have greater payload and altitude capability[5] and therefore larger and possibly less-constrained ballonets. This motivated simultaneous and independent re-examinations of the "frozen" ballonet assumption by Jones[6] and DeLaurier.[7] Jones envisioned the ballonet air as a fluid with a planar surface and used Lagrangian formulation to couple the ballonet fluid's motion to the system's dynamics. DeLaurier's analytical model and formulation are different, as shown in the next section, but the small perturbation forms of Jones' and DeLaurier's resulting dynamic equations are very similar. The main differences are in the treatment of ballonet slosh damping, and the assumption by Jones of negligible effect on the ballonet's dynamics by the vehicle's pitching acceleration $\dot{q}$, and that by DeLaurier of negligible effect from the vehicle's time rate of change of vertical relative velocity $\dot{w}$. Further, Jones' work was primarily directed toward refining a dynamic simulation for the study of a specific aerostat configuration in different flight conditions, whereas the purpose of this present analysis was to investigate the effects of ballonet design parameters, per se, on the dynamic stability of a typical aerostat.

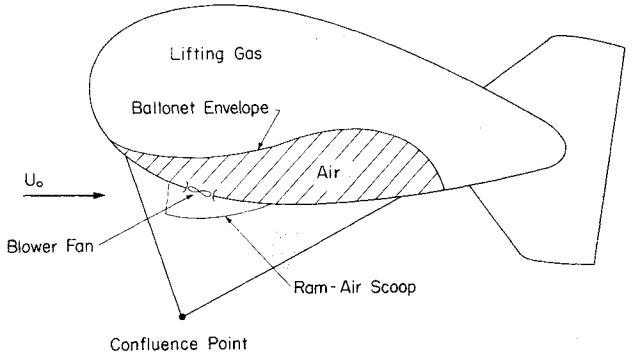


**Fig. 1 Schematic of typical ballonet.**

## Method of Analysis

### Analytical Model

The analytical model for the air and gas within the aerostat's hull draws on the fuel slosh research of NASA,[8] where it was found that a spring-mass-dashpot system gave an excellent model for the effects of fuel slosh on a rocket's dynamic stability. For this particular case, the concept was extended to account for the "slosh" of both the ballonet air and the gas. Hence, Fig. 3 shows lump masses for the air and gas, each of which are acted on by a spring and dashpot. Further, each mass is constrained to horizontal motion, and these motions are coupled by a fixed ratio (for a nonstretching hull). Note that there are no moment-of-inertia contributions with respect to the mass centers of the air and gas. Physically, this assumed that they are perfectly free to swirl within their volumes of containment.

The rest of the aerostat, including its confluence lines, is assumed to be perfectly rigid and acted on by a steady horizontal wind of speed $U_0$ and uniform density $\rho$. Also, since the ballonet is fullest at relatively low altitudes, the analysis will be restricted to those tether lengths $L$ for which

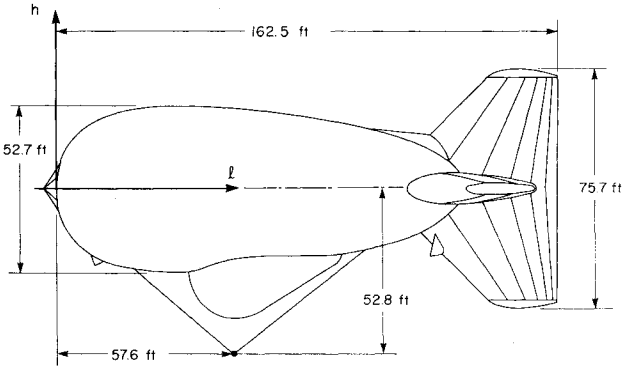


**Fig. 2 Model SN 204 Family-II aerostat.**

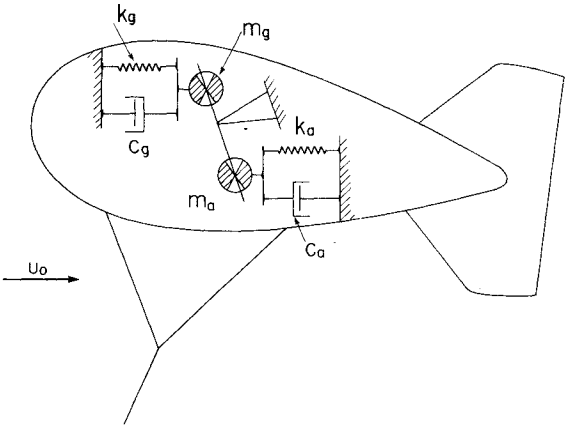


**Fig. 3 Analytical model for internal air and gas.**

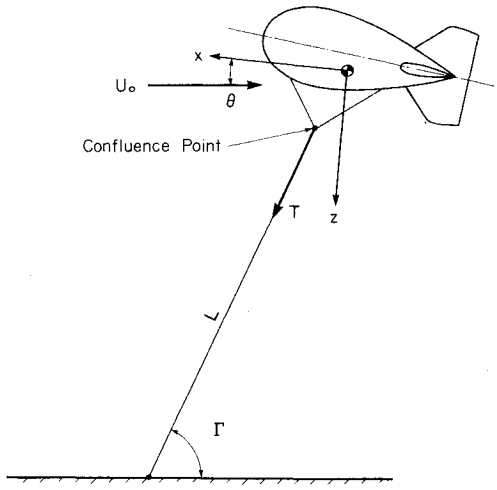


**Fig. 4 Coordinates for cable-aerostat system.**

the tether cable may be dynamically considered to be a massless, dragless rigid rod with frictionless pivots at the ground attachment point and the confluence point (Fig. 4). For large aerostats of the type currently in use[5] this restricts the validity of this analysis to tether lengths less than $\approx 1500$ ft.

Finally, since the purpose of this analysis is to study the system's stability with respect to a reference equilibrium configuration, the dynamic equations were linearized by means of a small perturbation analysis based on the following assumptions: 1) the magnitudes of the system's perturbed rotations are small, 2) the magnitudes of the aerostat's angular velocities are small compared with the ratio of $U_0$ to the aerostat's characteristic length $\bar{c}$, 3) the magnitudes of the system's perturbed velocities are small compared with $U_0$, and 4) aerodynamic forces and moments on the aerostat may be represented by the concept of stability derivatives.

**Formulation**

The basic idea behind this formulation is that the motion and gravity accelerations of the air and gas masses give rise to reaction forces and moments on the rest of the aerostat, and these may therefore be directly added to the force and moment terms in the dynamic equations of the cable-aerostat system, which are obtained in Ref. 3. In particular, the first-order reaction forces and moment of the ballonet air were calculated to be

$$\Delta X_a = -m_a[\dot{v}_a + \dot{u} + (z_a)_0\dot{q} + g\theta] \tag{1}$$

$$\Delta Z_a = -m_a[\dot{w} - U_0 q - (x_a)_0\dot{q}] \tag{2}$$

$$\Delta M_a = (z_a)_0\Delta X_a - (x_a)_0\Delta Z_a - m_a g\delta x_a \tag{3}$$

and similar equations were obtained for the contribution of the lifting gas.

The previously stated assumption of coupled motion gave

$$\delta x_g = \frac{-V_a}{V_g}\delta x_a, \quad v_g = \frac{-V_a}{V_g}v_a \tag{4}$$

which allowed the reaction force and moment equations of the air and gas to be added together and simplified:

$$\Delta X_a + \Delta X_g = -(m_a + m_g)\dot{u} - (m_a - m_g V_a/V_g)\dot{v}_a - [m_a(z_a)_0 + m_g(z_g)_0]\dot{q} - (m_a + m_g)g\theta \tag{5}$$

$$\Delta Z_a + \Delta Z_g = -(m_a + m_g)\dot{w} + (m_a + m_g)U_0 q + [m_a(x_a)_0 + m_g(x_g)_0]\dot{q} \tag{6}$$

$$\Delta M_a + \Delta M_g = -[m_a(z_a)_0 + m_g(z_g)_0]\dot{u} + [m_a(x_a)_0 + m_g(x_g)_0]\dot{w} - \{m_a[(x_a)_0^2 + (z_a)_0^2] + m_g[(x_g)_0^2 + (z_g)_0^2]\}\dot{q} - [m_a(x_a)_0 + m_g(x_g)_0]U_0 q - [m_a(z_a)_0 - m_g(z_g)_0 V_a/V_g]\dot{v}_a - [m_a(z_a)_0 + m_g(z_g)_0]g\theta - [m_a - m_g V_a/V_g]g\delta x_a \tag{7}$$

These terms may then be included with the first-order force and moment contributions of the cable, wind, buoyancy, and gravity to give, through the force acceleration equations of Etkin,[9] the first-order cable-aerostat dynamic equations:

$$\Delta X_a + \Delta X_g + \Delta X_c + \Delta X_{\text{aero}} + (B - mg)\theta = m\dot{u} \tag{8}$$

$$\Delta Z_a + \Delta Z_g + \Delta Z_c + \Delta Z_{\text{aero}} = m(\dot{w} - U_0 q) \tag{9}$$

$$\Delta M_a + \Delta M_g + \Delta M_c + \Delta M_{\text{aero}} + z_B B\theta = I_{yy}\dot{q} \tag{10}$$

where

$$\Delta X_c = (\cos\Gamma_0)\delta T - (T_0\sin\Gamma_0)(\theta + \gamma) \tag{11}$$

$$\Delta Z_c = (\sin\Gamma_0)\delta T + (T_0\cos\Gamma_0)(\theta + \gamma) \tag{12}$$

$$\Delta M_c = (z_{tp}\cos\Gamma_0 - x_{tp}\sin\Gamma_0)\delta T - T_0(z_{tp}\sin\Gamma_0 + x_{tp}\cos\Gamma_0)(\theta + \gamma) \tag{13}$$

and

$$\Delta X_{\text{aero}} = X_u u + X_{\dot{u}}\dot{u} + X_w w + X_{\dot{w}}\dot{w} + X_q q + X_{\dot{q}}\dot{q} \tag{14}$$

$$\Delta Z_{\text{aero}} = Z_u u + Z_{\dot{u}}\dot{u} + Z_w w + Z_{\dot{w}}\dot{w} + Z_q q + Z_{\dot{q}}\dot{q} \tag{15}$$

$$\Delta M_{\text{aero}} = M_u u + M_{\dot{u}}\dot{u} + M_w w + M_{\dot{w}}\dot{w} + M_q q + M_{\dot{q}}\dot{q} \tag{16}$$

Note that $m$ and $I_{yy}$ are inertial properties for the aerostat exclusive of $m_a$ and $m_g$, and the stability derivatives are referred to the mass center of $m$.

Four additional equations are obtained from the kinematic relations

$$v_a - (\dot{\delta x_a}) = 0 \tag{17}$$

$$q - \dot{\theta} = 0 \tag{18}$$

$$u + z_{tp}\dot{\theta} - (L\sin\Gamma_0)\dot{\gamma} = 0 \tag{19}$$

$$w - x_{tp}\dot{\theta} - U_0\theta + (L\cos\Gamma_0)\dot{\gamma} = 0 \tag{20}$$

and the mathematical statement is completed with the addition of the dynamic equation of the air and gas relative to the hull:

$$(m_a - m_g V_a/V_g)\dot{u} + [m_a(z_a)_0 - m_g(z_g)_0 V_a/V_g]\dot{q} + (m_a - m_g V_a/V_g)g\theta + \hat{M}\dot{v}_a + \hat{C}(\dot{\delta x_a}) + \hat{K}\delta x_a = 0 \tag{21}$$

where

$$\hat{M} \equiv m_a + m_g (V_a/V_g)^2 \tag{22}$$

$$\hat{C} \equiv c_a + c_g (V_a/V_g)^2 \tag{23}$$

$$\hat{K} \equiv k_a + k_g (V_a/V_g)^2 \tag{24}$$

Note that Eqs. (5-7, 17, 18, and 21) are the mathematical description of the internal air and gas dynamics of any lighter-than-air flight vehicle with a partially filled ballonet and an inextensible outer hull. These equations may therefore be utilized in the flight dynamic analysis of blimps as well as that for tethered aerostats.

#### Solution

Since the complete set of eight equations is first order and linear, they may be represented in the following matrix fashion:

$$[A] \begin{bmatrix} u \\ w \\ q \\ \theta \\ v_a \\ \delta x_a \\ \delta T \\ \gamma \end{bmatrix} - [E] \begin{bmatrix} \dot{u} \\ \dot{w} \\ \dot{q} \\ \dot{\theta} \\ \dot{v}_a \\ (\dot{\delta x_a}) \\ (\dot{\delta T}) \\ \dot{\gamma} \end{bmatrix} = 0 \tag{25}$$

where $[A]$ and $[E]$ are 8 × 8 matrices whose elements are the coefficients of the eight equations. With the assumption of a harmonic solution,

$$\begin{bmatrix} u \\ w \\ q \\ \theta \\ v_a \\ \delta x_a \\ \delta T \\ \gamma \end{bmatrix} \equiv \begin{bmatrix} \hat{U} \\ \hat{W} \\ \hat{Q} \\ \hat{\Theta} \\ \hat{V}_a \\ \hat{X}_a \\ \hat{T} \\ \hat{\Gamma} \end{bmatrix} e^{i\sigma t} \tag{26}$$

Equations (25) become the eigenvalue problem:

$$[A - \sigma E] \begin{bmatrix} \hat{U} \\ \hat{W} \\ \hat{Q} \\ \hat{\Theta} \\ \hat{V}_a \\ \hat{X}_a \\ \hat{T} \\ \hat{\Gamma} \end{bmatrix} = 0 \tag{27}$$

from which the eigenvalues $\sigma$ give the stability roots:

$$\sigma = \eta + i\omega \tag{28}$$

and the eigenvectors give the system's modal vectors.

## Application of Analysis

#### Ballonet Air Parameters

In the course of aerostat design and testing, the ballonet information that is most readily obtainable is the static mass center location of the ballonet air as a function of ballonet fullness $f$ and aerostat pitch angle $\theta$. It is useful, then, to express the air and gas spring constants $k_a$ and $k_g$ in terms of this information.

Note from the dynamic equations that $k_a$ and $k_g$ appear only once, and in the combination defined as $\hat{K}$ (Eq. 24). Therefore, a single value for $\hat{K}$ will completely account for the contributions of the two spring constants; this value is found from the static form of Eq. (21),

$$(m_a - m_g V_a/V_g) g\theta + \hat{K}\delta x_a = 0 \tag{29}$$

which gives

$$\hat{K} = \frac{(m_g V_a/V_g - m_a) g}{\mathrm{d}x_a/\mathrm{d}\theta} \tag{30}$$

This identifies the static constraint derivative, $\mathrm{d}x_a/\mathrm{d}\theta$, as a convenient parameter for characterizing the ballonet's fore-and-aft stiffness, with given $m_a$, $m_g$, and fullness.

Next, note that the damping coefficients, $c_a$ and $c_g$, also appear in a single combination defined as $\hat{C}$ (Eq. (23)). An expression for this may be found from the unforced (no aerostat hull motion) form of Eq. (21):

$$\hat{M}\dot{v}_a + \hat{C}(\delta x_a) + \hat{K}\delta x_a = 0 \tag{31}$$

which, with Eq. (17), gives the classical spring-mass-dashpot equation. Therefore,

$$\hat{C} = \frac{0.2206\,(\hat{K}\hat{M})^{1/2}}{[(N_{1/2})^2 + 0.01217]^{1/2}} \tag{32}$$

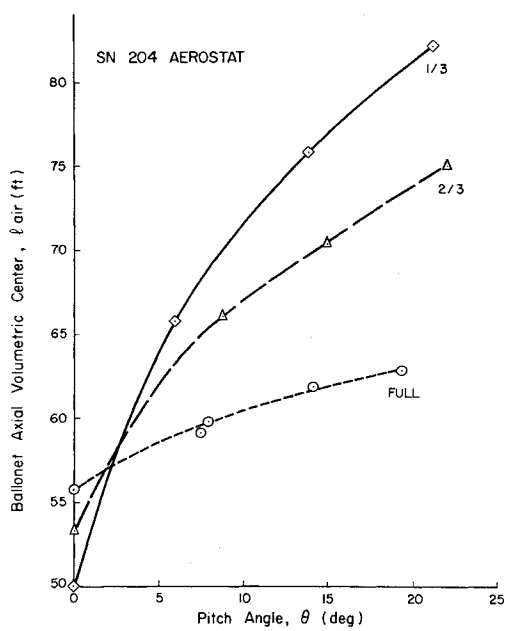


**Fig. 5 Ballonet axial volumetric center location.**

which identifies the number of cycles to half amplitude $N_{1/2}$ as a convenient parameter for characterizing the ballonet's fore-and-aft damping, with given $m_a$, $m_g$, fullness, and stiffness.

**Numerical Example**

The 200,000 ft$^3$ Family-II aerostat (Fig. 2) is representative of recent tethered aerostat designs, and hence it is a suitable example for showing the dynamic effects of ballonet slosh. The specific Family-II aerostat chosen is the SN 204 model, which was thoroughly tested and measured by the RCA TELTA personnel under the direction of the U.S. Air Force's Range Measurements Laboratory. Its physical characteristics are given in Ref. 10, from which the ballonet mass-center plots in Figs. 5 and 6 were calculated.

Further, a baseline reference case was chosen for which:

$L = 1000$ ft $\qquad U_0 = 25$ knots (42.2 ft/s)

$m_g = 73.5$ slugs $\qquad$ Helium purity = 98%

From this, and polynomial curve-fit equations to Fig. 5, it was calculated that

$m_a = 69.4$ slugs $\qquad V_a = 30{,}037$ ft$^3$

$V_g = 173{,}962$ ft$^3$ $\qquad f = 47.7\%$

$l_a = 68.0$ ft $\qquad h_a = -22.9$ ft

$l_g = 56.3$ ft $\qquad h_g = 3.9$ ft

$$dx_a/d\theta = -73.4 \text{ ft/rad}$$

The inertial properties for the rest of the aerostat were:

$m = 319.7$ slugs $\qquad l_{cm} = 85.2$ ft

$h_{cm} = -9.56$ ft $\qquad I_{xx} = 95{,}901.9$ slug-ft$^2$

$I_{yy} = 938{,}753.9$ slug-ft$^2$

$I_{zz} = 898{,}635.0$ slug-ft$^2$

$I_{xz} = -8{,}423.9$ slug-ft$^2$

The equilibrium pitch angle for this particular case was 7.8 deg, for which the following nondimensional stability derivatives were calculated in accordance with the wind tunnel data of Haak[11] and the estimation techniques of Ashley.[12]

| | | | | | |
|---|---|---|---|---|---|
| $C_{x_0}$ | $= -0.153$ | $C_{z_0}$ | $= -0.395$ | $C_{m_0}$ | $= 0.021$ |
| $C_{x_u}$ | $= 0.0$ | $C_{z_u}$ | $= 0.0$ | $C_{m_u}$ | $= 0.0$ |
| $C_{x_{\dot{u}}}$ | $= -0.240$ | $C_{z_{\dot{u}}}$ | $= 0.0$ | $C_{m_{\dot{u}}}$ | $= 0.023$ |
| $C_{x_\alpha}$ | $= -0.240$ | $C_{z_\alpha}$ | $= -3.053$ | $C_{m_\alpha}$ | $= -0.008$ |
| $C_{x_{\dot{\alpha}}}$ | $= 0.0$ | $C_{z_{\dot{\alpha}}}$ | $= -1.320$ | $C_{m_{\dot{\alpha}}}$ | $= 0.245$ |
| $C_{x_q}$ | $= 0.025$ | $C_{z_q}$ | $= -1.262$ | $C_{m_q}$ | $= -0.925$ |
| $C_{x_{\dot{q}}}$ | $= 0.046$ | $C_{z_{\dot{q}}}$ | $= 0.490$ | $C_{m_{\dot{q}}}$ | $= -0.173$ |

The dimensional stability derivatives of Eqs. (14-16) may be obtained from Ref. 12, where the reference area $S = 3465$ ft$^2$ and the reference length $\bar{c} = 138$ ft.

Further, the properties of the aerostat's total displaced volume (molded volume, in naval architectural terms) are $V_{\text{total}} = 248{,}400$ ft$^3$, $l_v = 70.08$ ft, $h_v = -0.79$ ft from which the total buoyant force was calculated to be $B = \rho g V_{\text{total}} = 18{,}486.6$ lb.

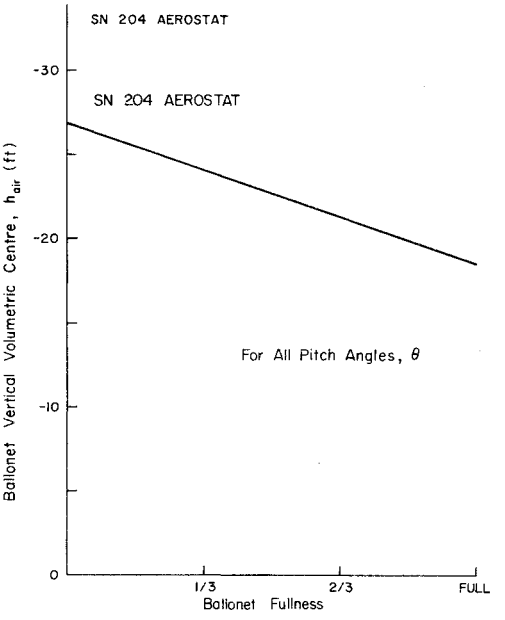


**Fig. 6 Ballonet vertical volumetric center location.**

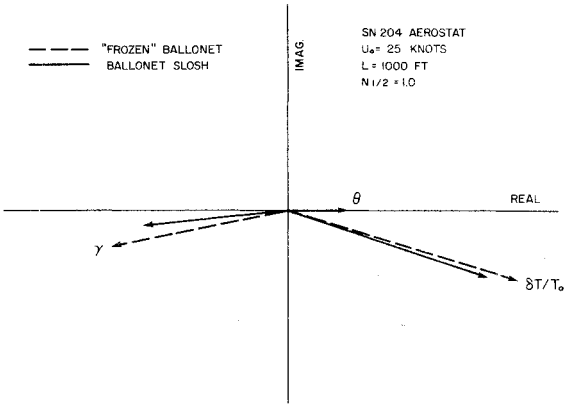


**Fig. 7 Vector diagram of first mode.**

Finally, the value chosen for the baseline damping parameter was $N_{1/2} = 1$. This was obtained from experiments by Holt[4] on a dynamically scaled model of the SN 204's hull and ballonet. It should be noted that no other quantitative data on ballonet slosh damping are available, and that the above value is an order-of-magnitude approximation.

**Results for Example**

The first step in this investigation was to compare the calculated dynamic stability of the SN 204 with that predicted by the stability analysis of Ref. 3, which assumed a "frozen" ballonet. Figure 7 shows that the modal vector for the first mode of motion (the upside-down pendulum mode) is relatively unaffected by ballonet slosh. The notable differences are that the ratio of pitch $\theta$ to surge $\gamma$ increased by about 17%, and $\gamma$ is more nearly 180 deg out of phase with $\theta$. Also, the stability roots remained essentially unchanged:

"frozen" ballonet:
$\eta = -0.0359$/s, $\quad \omega = 0.1003$ rad/s

ballonet slosh:
$\eta = -0.0358$/s, $\quad \omega = 0.1003$ rad/s

The second mode (the "pure-pitching" mode) was much more affected. Figure 8 shows that the tether tension variation $\delta T/T_0$ changes magnitude by 32% and phase by 22 deg. Also,

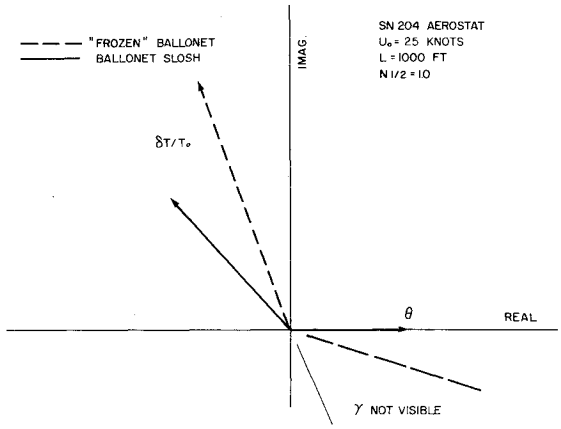


Fig. 8 Vector diagram of second mode.

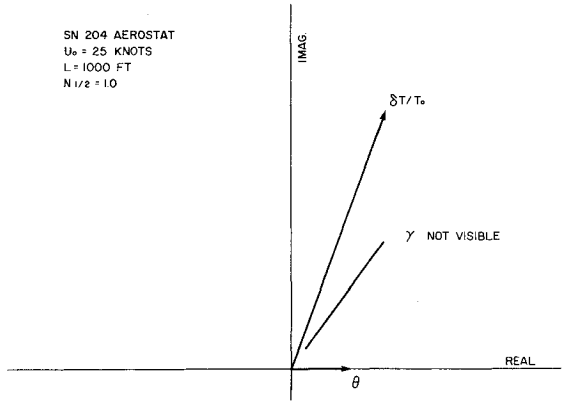


Fig. 9 Vector diagram of third mode.

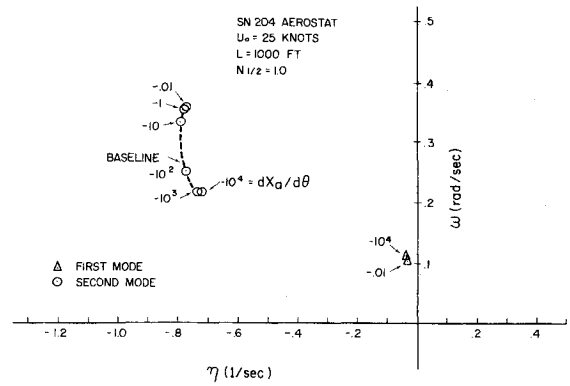


Fig. 10 Roots locus of 1st and 2nd modes with $dx_a/d\theta$ variation.

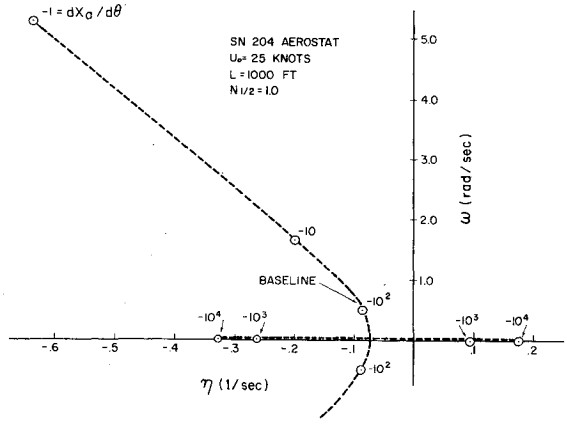


Fig. 11 Roots locus of 3rd mode with $dx_a/d\theta$ variation.

the surge phase changes by 48 deg, although for both cases the magnitudes are negligible. A comparison of the stability roots shows that damping is relatively unchanged, but that frequency decreases to half its original value:

"frozen" ballonet:
$\eta = -0.7164/s, \quad \omega = 0.4362$ rad/s

ballonet slosh:
$\eta = -0.7731/s, \quad \omega = 0.2615$ rad/s

Compared with the frozen ballonet case, the introduction of ballonet slosh in the physical model gave an additional degree of freedom which, in turn, gave two additional stability roots with their corresponding modal vectors. For this specific case the roots were complex conjugates, and the "third mode" modal vector is shown in Fig. 9. As with the second mode, the motion is nearly pure pitching, although the magnitudes and phases of the other two vectors are considerably different. In particular, the magnitude ratio of $\delta T/T_0$ to $\theta$ is nearly twice that for the second mode, and $\delta T/T_0$ lags the second mode's $\delta T/T_0$ by 40 deg. The frequency and damping are also considerably different:

$$\eta = -0.0896/s, \qquad \omega = 0.6043 \text{ rad/s}$$

Although this mode is stable, it is evident that its degree of stability is of the same order of magnitude as that for the first mode which, as was stated in the Introduction, has been considered to be the least stable and most important mode for design purposes. Clearly, the third mode warrants the same attention.

The next step in the investigation was a study of the effect of changing $dx_a/d\theta$ from $-0.01$ to $-10^4$ ft/rad. This corresponds to a change from essentially the "frozen" ballonet case to one where the ballonet air has very little fore-and-aft constraint. All other parameters were held fixed at the previous values.

Figure 10 shows the effect on the first and second mode stability roots, where one sees that the first mode values are scarcely affected, whereas the frequency of the second mode roots is nearly halved in going from $dx_a/d\theta = -0.01$ to $-10^4$. The change in damping, however, is less than 6%, and it is clear that neither of these modes are driven to instability by the introduction of ballonet slosh.

The effect on the third mode root is very different, as seen in Fig. 11. With increasing magnitudes of $dx_a/d\theta$, the damping rapidly decreases until instability is reached at $dx_a/d\theta \approx -300$ ft/rad. Since the SN 204's value for this case is $-73.4$ ft/rad, its third mode root is safely stable. However, from Figs. 5 and 6, the maximum attainable value of $dx_a/d\theta$ is over $-700$ ft/rad when pitch angle equals 0 deg and fullness equals 1/3. This is not a condition that is attainable for the SN 204 within its normal flight envelope, but it does show that considerably high magnitudes of $dx_a/d\theta$ are possible for an actual ballonet design.

Finally, the effect of $N_{1/2}$ on the baseline system's stability was investigated. With all other parameters held constant, including $dx_a/d\theta$, $N_{1/2}$ was varied from 0.5 to 100, which corresponds to a change from half the baseline value to that for an extremely (and unrealistically) undamped ballonet. This large variation scarcely affected the stability roots of the first and second modes, as may be seen in Fig. 12; but as shown in Fig. 13, the effect on the third mode's stability is much greater. With increasing $N_{1/2}$ from the baseline value, the third mode becomes less stable, as one would expect; but it never goes unstable, even with the extremely undamped value of $N_{1/2} = 100$. Moreover, increasing the damping to $N_{1/2} = 0.5$ nearly doubled the third mode's stability, which indicates that

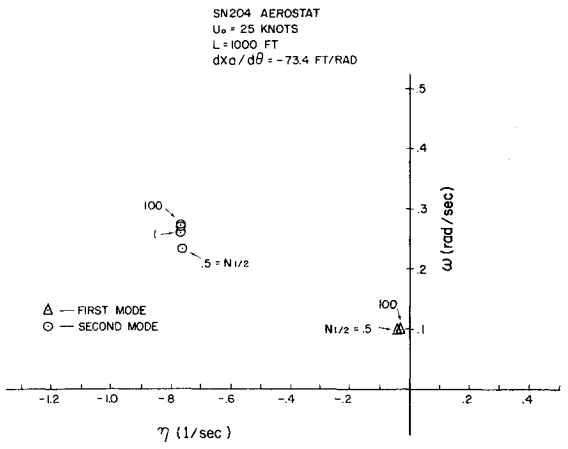


**Fig. 12 Roots locus of 1st and 2nd modes with $N_{1/2}$ variation.**

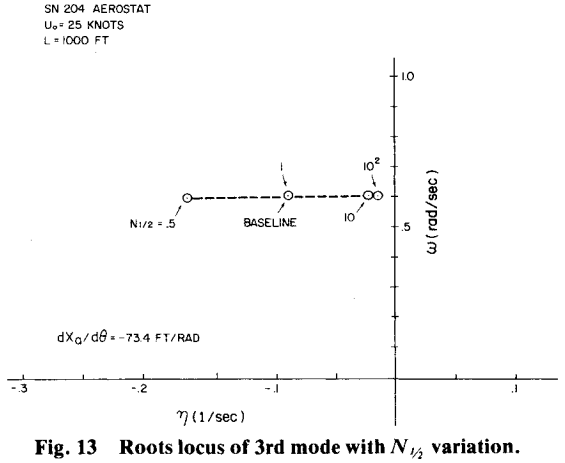


**Fig. 13 Roots locus of 3rd mode with $N_{1/2}$ variation.**

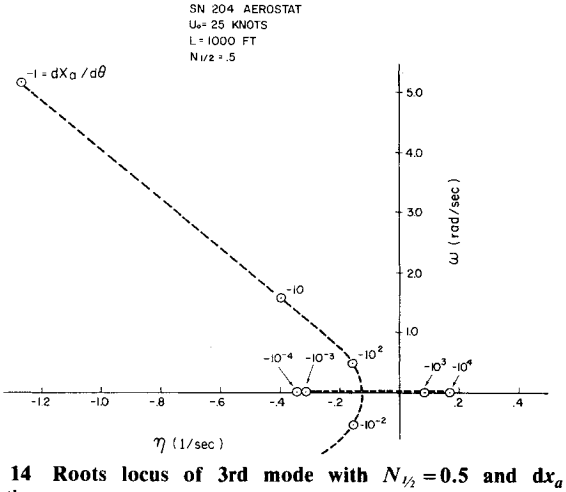


**Fig. 14 Roots locus of 3rd mode with $N_{1/2} = 0.5$ and $dx_a/d\theta$ variation.**

decreased ballonet damping does not necessarily drive the system unstable, and relatively small increases in damping may significantly increase the system's stability.

A further look at the influence of damping is provided by Fig. 14, where $dx_a/d\theta$ was varied from $-1$ to $-10^4$, and $N_{1/2}$ was fixed at 0.5. One sees that the third mode now goes unstable at $dx_a/d\theta \approx -450$ ft/rad, which is an increase of 50% over the baseline case (Fig. 11). Again, this shows that increased slosh damping improves the system's stability.

## Conclusions

The results from the specific numerical example indicate that an aerostat's internal air and gas dynamics do not significantly affect the system's first ("upside-down pendulum") mode. This bears out the "frozen ballonet" assumption of the stability analyses in Refs. 1-3. Also, although the second ("pure-pitching") mode is somewhat more affected, it still remains very heavily damped compared with the first mode. However, the internal air and gas motions give additional modes (two complex conjugate or two real roots) which may have the same degree of stability, or less, as the first mode. This shows that improper ballonet design may result in a tethered aerostat system whose longitudinal stability is significantly worse than that predicted by the analyses of Refs. 1-3.

For the analytical model chosen in this research, it was shown that convenient parameters for dynamically characterizing the internal air and gas are $dx_a/d\theta$ and $N_{1/2}$, where $dx_a/d\theta$ is a measure of the ballonet's longitudinal constraint and $N_{1/2}$ is a measure of its damping. Further, it was shown, with reference to the baseline numerical example, that a tethered aerostat's stability decreases with decreasing ballonet constraint and damping, and that a low enough constraint could drive the third mode, and hence the system, unstable.

If the hull and ballonet fabric are nonstretching, as was assumed for this analysis, the ballonet's constraint depends entirely upon the geometry of the ballonet's envelope and that portion of the hull beneath it (Fig. 1). In particular, the "flatter" the longitudinal curve of the hull portion, the less constrained the ballonet air will be (like water in a plate, instead of a bowl). For that reason, aerostat configurations with larger hull fineness ratios than the Family-II design, or hull midsections which are right circular cylinders, could have poor longitudinal stability under certain operational conditions.

Also, the current design practice of configuring the full inflated ballonet as a long single chamber gives minimal longitudinal slosh damping for the partially inflated case. This situation, as well as the constraint problem, would be further aggravated for future aerostats with higher operational altitudes because the maximum ballonet volume would be a higher percentage of the total hull volume.

This research has shown that a tethered aerostat may have serious stability problems if insufficient consideration is given to the constraint and damping of its ballonet. However, what has also been shown is that values of constraint and damping which seem reasonably achievable from a design standpoint will strongly stabilize the third mode. In particular, consideration should be given to design measures such as: 1) "deep-bellied" hulls below the ballonet chamber, 2) multiple ballonets, 3) ballonet curtains stayed with internal lines, and 4) coarse-woven antisurge curtains within the ballonet.

## Acknowledgment

This work was financially supported by a grant entitled "Tethered Aerostats with Maximized Stability" from the National Research Council of Canada.

## References

[1] Doyle, G.R. and Vorachek, J.J., "Investigation of Stability Characteristics of Tethered Balloon Systems," AFCRL-71-0406, July 30, 1971, Air Force Cambridge Research Laboratories, Bedford, Mass.

[2] DeLaurier, J.D., "A Stability Analysis for Tethered Aerodynamically Shaped Balloons," *Journal of Aircraft*, Vol. 9, Sept. 1972, pp. 646-651.

[3] DeLaurier, J.D., "Refinements and Experimental Comparisons of a Stability Analysis for Aerodynamically-Shaped Tethered Balloons," AIAA Paper 75-943, Snowmass, Colo., July 1975.

[4]Holt, C.F., "Ballonet Gas Motion in Large Balloons," *Proceedings, Eighth AFCRL Scientific Balloon Symposium*, Aug. 21, 1974, pp. 189-201.

[5]Arnold, E.M., "Tethered Aerostats Used in TCOM Systems," AIAA Paper 77-330, AIAA 13th Annual Meeting, Washington, D.C., Jan. 10-14, 1977.

[6]Jones, S.P., "The Motion of Ballonet Air Affecting the Dynamic Stability of Tethered Aerostats," TCOM Corp., Columbia, Md., to be published.

[7]DeLaurier, J., "An Investigation of the Effect of Ballonet Motions on Tethered-Aerostat Longitudinal Dynamic Stability," UTIAS Tech. Note No. 205, May 1977, University of Toronto, Institute for Aerospace Studies, Downsview, Ontario.

[8]Bauer, H.F., "Vehicle Stability and Control," *The Dynamic Behavior of Liquids in Moving Containers*, NASA SP-106, edited by H. Norman Abramson, 1966, pp. 225-267.

[9]Etkin, B., "General Equations of Unsteady Motion," *Dynamics of Flight*, 5th ed., Wiley, New York, 1966, pp. 94-144.

[10]"Design Verification of the IID-7A Balloon," TR 74-058, Vol. 1, Aug. 31, 1974, Range Measurements Laboratory, Patrick Air Force Base, Fla.

[11]Haak, E.L., "Wind Tunnel Test Results—Family II-D Aerodynamically Shaped Balloon," SER 0093, March 1971, G. T. Schjeldahl Co., Northfield, Minn.

[12]Ashley, H., "Small-Perturbation Response and Dynamic Stability of Flight Vehicles," *Engineering Analysis of Flight Vehicles*, Addison-Wesley, Reading, Mass., 1974, pp. 173-205.